THE ASTROPHYSICAL JOURNAL, Vol. 151, January 1968

NEUTRAL HYDROGEN OBSERVATIONS OF THE BINARY GALAXY SYSTEM NGC 4631/4656

MORTON S. ROBERTS
National Radio Astronomy Observatory,* Green Bank, West Virginia
Received June 9, 1967; revised July 3, 1967

ABSTRACT

A link or "bridge" of neutral atomic hydrogen connecting the galaxies NGC 4631 and NGC 4656 is described. The galaxies are separated by 0°.5. At a distance of 4 Mpc, the minimum separation of their centers is 38 kpc. The systemic radial velocities of the two galaxies agree to within ~30 km/s. The hydrogen content for the entire system is $6.1 \times 10^9 M\odot$, of which $0.7 \times 10^9 M\odot$ is associated with the bridge. Ten of the observed drift curves for NGC 4631 can be satisfactorily reproduced by a set of drift curves generated from a model galaxy that is convolved with the observing antenna beam. Such a procedure yields a rotation curve as well as the distribution and random motions of the hydrogen. The best fitting model has a random motion term of 30 km/s. These data yield an estimate of the average optical depth for this nearly edge-on system. Several of the drift curves, corresponding to velocities of the east end of the galaxy, are only poorly reproduced by the model. They are better matched if an expansion term is included in the analysis. However, any adopted model is not necessarily a unique representation of the data. The adopted rotation curve indicates a total mass for NGC 4631 of $6.8 \times 10^{10} M\odot$; the neutral hydrogen is 6 per cent of the total mass.

No satisfactory model for NGC 4656 could be found, although a systemic radial velocity of about 600 km/s is indicated. A rough estimate of the total mass of this system is $1.5 \times 10^{10}/\sin^2 i\ M\odot$. The fractional hydrogen content is $0.09 \sin^2 i$.

I. INTRODUCTION

The late-type spiral NGC 4631 is of special interest for 21-cm hydrogen studies because of its large angular size and edge-on aspect. Under favorable circumstances this geometry will yield information on possible neutral hydrogen in the halo regions of a galaxy (Roberts 1966). A measurable amount of halo hydrogen would be evidenced in the integrated brightness temperature contours; a profile perpendicular to the major axis would be broader than the antenna-beam pattern. Initial observations showed such a broadening in the H I contours of NGC 4631, and a confirming set of observations was obtained during a second observing period. In both cases the contour profiles were asymmetrical, being more extended to the south. To map this region further, a third set of observations was obtained south of NGC 4631 extending to and beyond NGC 4656. The latter galaxy is $\frac{1}{2}°$ southeast of NGC 4631; the systemic radial velocities for these two systems differ by about 30 km/s. The third set of 21-cm observations showed that the southern extension of NGC 4631, referred to above, continued to NGC 4656 and merged with the H I contours for this latter system. The suggestion in the initial data of an H I halo referred instead to an H I bridge between the two galaxies.

Such a feature is not unique, as a similar link appears between the Small and Large Magellanic Clouds (Hindman, Kerr, and McGee 1963). The distance between the cloud centers is 27 kpc, for distance moduli of 18.7 and 19.0 for the LMC and SMC, respectively (Bok 1966). At a distance of 4.0 Mpc, the minimum separation between NGC 4631 and 4656 is 38 kpc. Structural types of Irr I and Sm have been assigned to NGC 4656; its appearance is that of a distorted spiral (see Fig. 2, Pl. 6). The hydrogen bridge marks the pair NGC 4631/4656 as a physically related binary system, which in turn may account for the peculiar appearance of NGC 4656.

A third galaxy, NGC 4627, lying 1′ north of NGC 4631, may also be related to the

* Operated by Associated Universities, Inc., under contract with the National Science Foundation.

PLATE 6

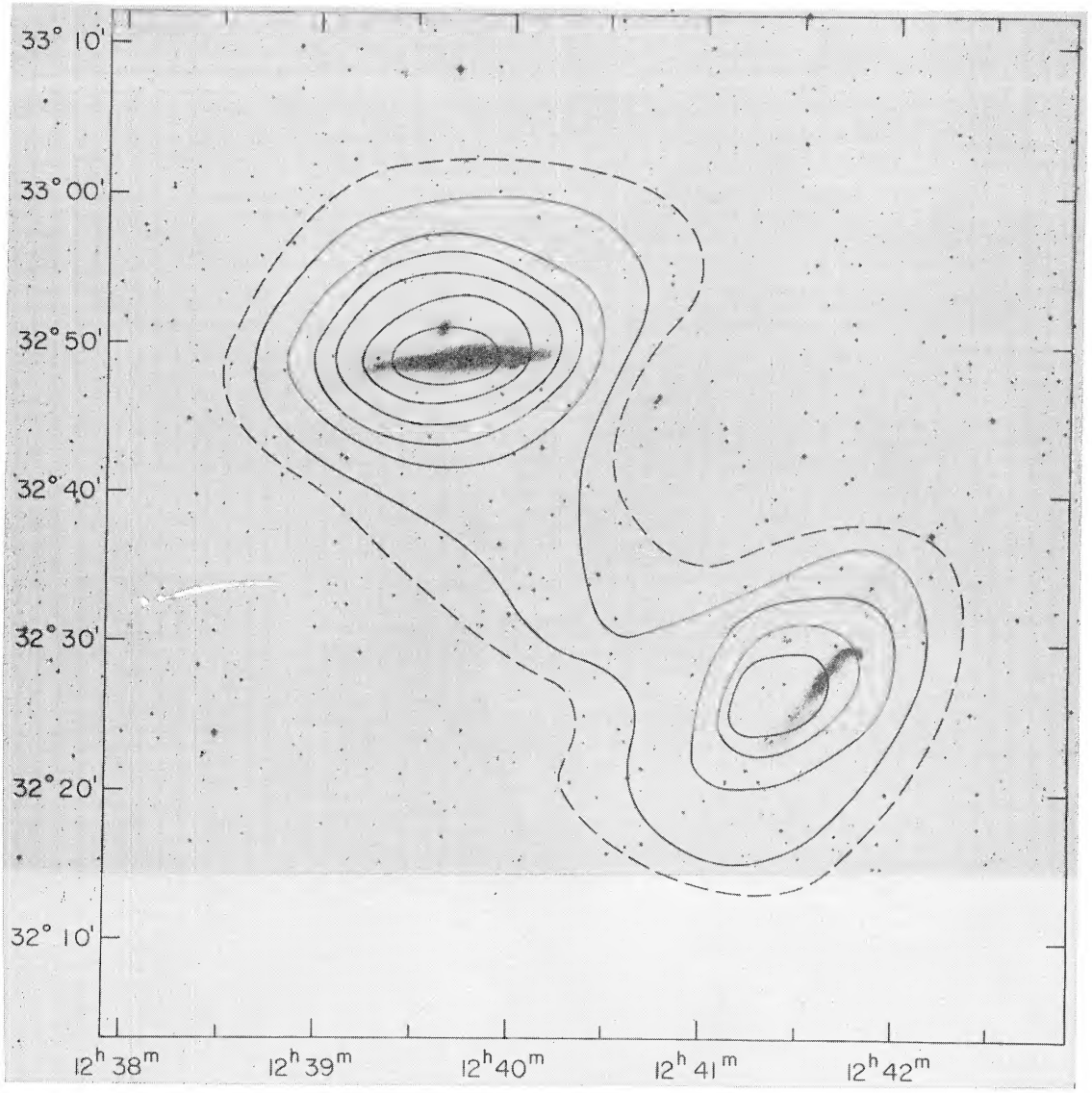

FIG. 2.—The contours of Figure 1 superimposed on a 48-inch Schmidt *Sky Survey* photograph of the region

physical pair NGC 4631/4656. Only optical evidence is available here. The appearance of globular clusters in NGC 4627 suggests that it is relatively close and not just a chance coincidence with a distant background galaxy (Sandage 1961). No radial velocity is available for NGC 4627. Arp (1966) has included NGC 4631/4627 in his *Atlas of Peculiar Galaxies* and calls attention to a "diffuse counter tail" on NGC 4627. The *New General Catalogue* lists a fourth object in this region, NGC 4657. It is a high surface brightness feature at the northeast end of the bar that defines NGC 4656 and is most likely a part of NGC 4656.

The observations reported here were obtained with the 300-foot telescope, which has a beam size of 10′ to half-intensity. The known antenna pattern will not admit beam smearing or side-lobe confusion as possible instrumental effects responsible for the H I bridge. An added discriminant against such instrumental confusion is present since these data refer to spectral line observations.

The neutral atomic hydrogen distribution and content for the NGC 4631/4656 system are presented below. In addition, the kinematics within the two systems are discussed. A model-fitting program has been applied to the data for NGC 4631 and a rotation curve and total mass are derived. An estimate for the total mass of NGC 4656 is also given.

II. DISTANCE

The group membership and distance of NGC 4631/4656 are subject to some uncertainty and confusion. Using the diameters of H II regions, Sersic (1960) placed NGC 4631 in the Ursa Major II Group and NGC 4656 in the Ursa Major I Group. The distances he assigned to these groups are 5.2 and 3.3 Mpc, respectively. These two groups lie in the region of and contain members in common with the Canes Venatici Cluster as defined by van den Bergh (1960). From galaxy luminosity criteria, van den Bergh derived a distance of 4.4 Mpc for this cluster. NGC 4631 is specifically assigned to the CVn Cluster. This distance of 4.4 Mpc was adopted by de Vaucouleurs and de Vaucouleurs (1963) in their optical study of NGC 4631. In a later discussion of groups of galaxies de Vaucouleurs (1966) places NGC 4631 and NGC 4656 in the CVn II Cloud and assigns a distance of 8.0 Mpc to this cloud. CVn II Cloud membership is similar to Sersic's Ursa Major II Group, while de Vaucouleurs' CVn I Cloud, at a distance of 3.8 Mpc, is similar to Sersic's Ursa Major I Group.

Corrections to the distance scales adopted by Sersic and van den Bergh have been proposed by Sandage (1962). In addition, de Vaucouleurs (1966) has recalibrated van den Bergh's luminosity classes and derives slightly different absolute magnitudes. However, with a range of distances of 3.3–8.0 Mpc for the NGC 4631/4656 system already available, these later changes are minor. With the exception of the suggested membership in the CVn II Cloud at a distance of 8.0 Mpc, the various distance estimates for NGC 4631/4656 lie close to 4 Mpc. We shall adopt this value in the following discussion. The errors quoted for distance-dependent parameters derived below do not include the uncertainty in the distance.

III. OBSERVATIONS

All observations were made with the 300-foot telescope and a 20-channel receiver (Höglund and Roberts 1965), having filter widths of 95 kHz spaced 100 kHz center to center. The receiver output was recorded in both analogue and digital forms. The analogue records were used to monitor possible interference or equipment malfunction; the digital data were used in the averaging and reduction analysis. The final output was displayed as a series of drift curves; velocity profiles were generated from these drift curves for various points over the region studied.

The data were obtained over three observing periods with enough overlap to insure a proper tie-in of the data sets. The over-all system noise was 250° K in the first two peri-

ods. An improved parametric amplifier gave a 200° K system temperature for the third set of observations. The beam efficiency of the 300-foot telescope was 53 per cent for the first observing period and 48 per cent during the last two observing periods.

IV. HYDROGEN DISTRIBUTION

Figure 1 displays contours of 21-cm line radiation from the NGC 4631/4656 system. These contours are of the summation $\Sigma_i(\langle T_B \rangle)_i \Delta v_i$ and represent the beam-averaged brightness temperature, $\langle T_B \rangle$, integrated over all velocity filters, Δv. The H I link between the two galaxies is clearly outlined by the 100° K (km/s) contour. The 100-level

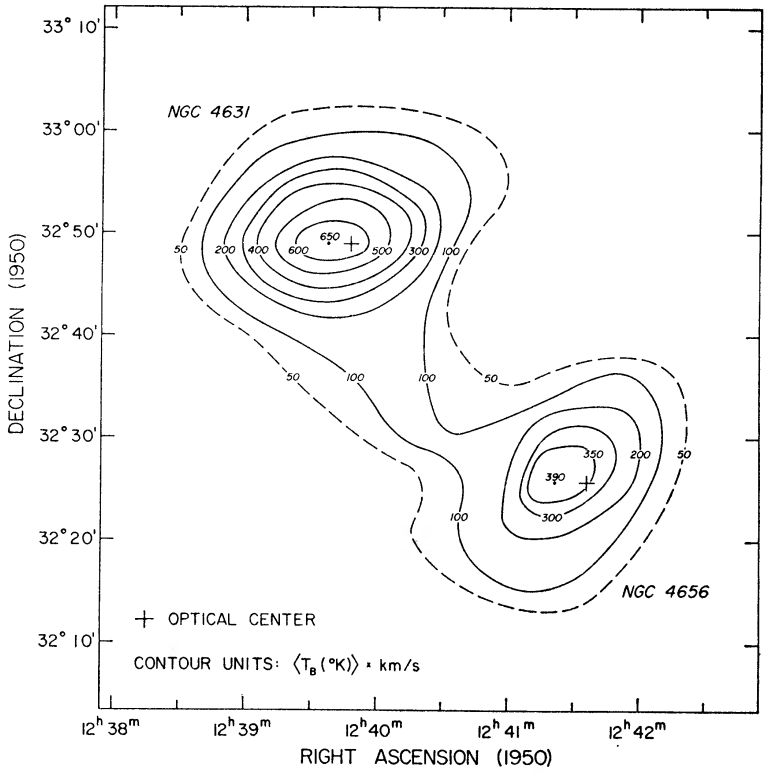

FIG. 1.—Contours of beam-averaged integrated brightness temperature for the NGC 4631/4656 system.

contour appears to pinch together near the southern end of the bridge. If this feature is real, an alternative explanation for the appearance of the H I contour bridge is possible. This would involve two hydrogen bulges or jets extending toward each other, one from each galaxy. Antenna beam smearing over this smaller region could then yield the continuous contours shown in Figure 1. In the following we will consider only the geometrically simpler case of a single connecting H I link between NGC 4631 and NGC 4656. The contours are shown again in Figure 2 (Plate 6) superimposed on a photograph of NGC 4631/4656.

From the known angular separation of the two galaxies, we may estimate the length of the bridge. By assuming that both systems are at the same distance, we obtain a minimum value of 38 kpc. The width of the bridge is far less certain because of beam-smearing effects. Only two contours define the bridge and the exact placing of the faintest contour, 50° K (km/s), is uncertain because of the poor signal-to-noise ratio. To emphasize the uncertainty, this contour is drawn as a dashed line in Figures 1 and 2. The ob-

served width of the bridge at half-intensity averages 15′. For a Gaussian distribution of radiation this would correspond to a true half-width of 11′ or 13 kpc. If the shape of the bridge is approximated by a cylinder of the above dimensions, its volume is 1.5×10^{68} cm^3.

The mass of neutral atomic hydrogen is given by

$$\frac{M_{\mathrm{H\,I}}}{M_\odot} = 1.236 \times 10^3 D^2 C \iiint [T_B(\theta,\phi,v)]\, d\theta\, d\phi\, dv\,, \qquad (1)$$

where D is the distance in megaparsecs. The factor C is included to allow for a possible non-negligible optical depth (see § VII below) and as used in equation (1) represents an average for the entire galaxy. If the system is optically thin, this factor is unity. The integration is over the beam-convolved H I distribution in arc minutes and over velocity in km/s. Table 1 lists the H I masses derived. Two entries are given for NGC 4631; the higher value for $M_{\mathrm{H\,I}}$ includes a correction for the optical depth.

The average projected surface density of H I in the bridge region is 0.06 atom cm^{-3} kpc. To estimate the volume density we may consider two cases: a cylinder of the above dimensions (38 × 13 kpc) and a thin sheet 0.5 kpc thick. The respective densities are

TABLE 1

NEUTRAL HYDROGEN MASSES*

Object	$M_{\mathrm{H\,I}}$ ($10^9 M_\odot$)
NGC 4631:	
Optically thin case	3 0
Corrected for opacity	4 0
NGC 4656	1 4
Bridge	0 7
Entire system (with corrected NGC 4631)	6 1

* The estimated uncertainty is 15 per cent.

then 0.006 and 0.11 atom/cm^3. For comparison, estimated average H I number densities for galaxies of different structural type are (Roberts 1963): Irr, 1.4; Sc, 0.9; Sb, 0.4 (atom/cm^3).

The peak as well as the point of symmetry of the observed H I distribution for both NGC 4631 and NGC 4656 show significant displacements from the Shapley-Ames positions for the optical centers of these systems. For NGC 4631 the H I is displaced 2′.2 west with respect to the optical center; for NGC 4656 the displacement is 3′.0 west. These shifts are much larger than the pointing correction errors for the 300-foot telescope and the usual uncertainties associated with optical galaxian coordinates. A smaller shift, but one in the same sense, has been derived for NGC 4631 by de Vaucouleurs and de Vaucouleurs (1963). To obtain a symmetrical rotation curve from optical radial velocity measurements of NGC 4631, they require a shift of 40″ west with respect to a luminosity distribution feature they associate with a bar seen end-on (de Vaucouleurs and de Vaucouleurs 1963, Fig. 3).

Radio continuum observations (Heeschen and Wade 1964) also indicate a displacement to the west of the catalogue value for the optical center of NGC 4631. The difference here is 0′.9. Similar continuum observations indicate that the radio center of NGC 4656 is 2′.3 east of the optical center. However, the radio measurements for NGC 4656 at both 750 MHz and 1400 MHz are very uncertain, and this suggested eastward displacement is of corresponding low weight. This is not the case for NGC 4631, which has a relatively high antenna temperature for a normal galaxy.

The largest displacement for NGC 4631 is found in the H I data. This is consistent

with the suggestion that this galaxy is a Magellanic-type system seen edge-on with the prominent single arm lying west of the center (de Vaucouleurs and de Vaucouleurs 1963, Fig. 8).

V. VELOCITY MEASUREMENTS

Velocity profiles for NGC 4631, NGC 4656, and the bridge region are shown in Figures 3–5. For NGC 4631 the velocity profiles are along selected regions of the major axis. The western part of the galaxy is approaching. The velocity profiles for NGC 4656

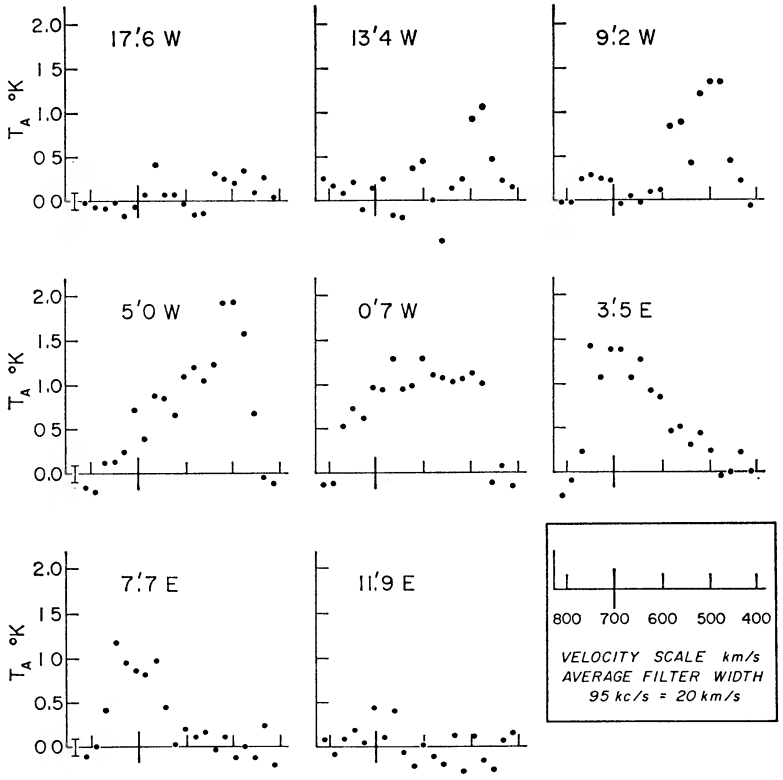

FIG. 3.—Velocity profiles along the major axis of NGC 4631. The error bars at the left of the figure show the rms error for an individual point. The heavy vertical line on the velocity axis of each profile corresponds to 700 km/s.

are on or close to the major axis. The read-out rate for digital data recording was $10^s = 2'.1$; this quantizes the positions at which velocity profiles may be constructed. Figure 5 displays a series of velocity profiles starting at the center of NGC 4631 and extending through the bridge region to the center of NGC 4656; the positions indicated in this figure are with respect to the optical center of NGC 4631. The approximate region of the bridge is outlined by a dashed line. The rms error bars for an individual point are shown to the left of each row.

The velocity profiles in Figure 5 provide two tests on the possibility that the bridge is due to antenna-beam smearing. These are (1) the strength of the signal at various distances from the galaxies; and (2) the radial velocity field in the bridge region compared to that in the galaxies. The first column of velocity profiles in Figure 5 is at a common right ascension and at various declinations south of NGC 4631. In this series the closest distance to NGC 4656 is $\sim 23'$. At the center of NGC 4631, the velocity

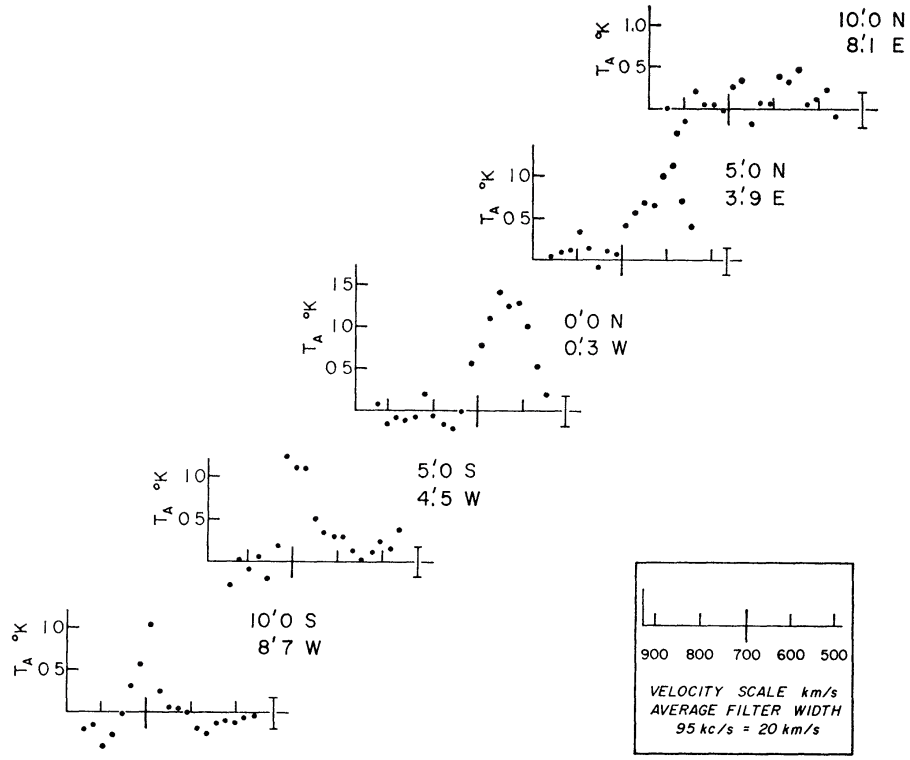

FIG. 4.—Velocity profiles along the major axis of NGC 4656. The rms error bar is for an individual point. The heavy vertical line on the velocity axis of each profile corresponds to 700 km/s.

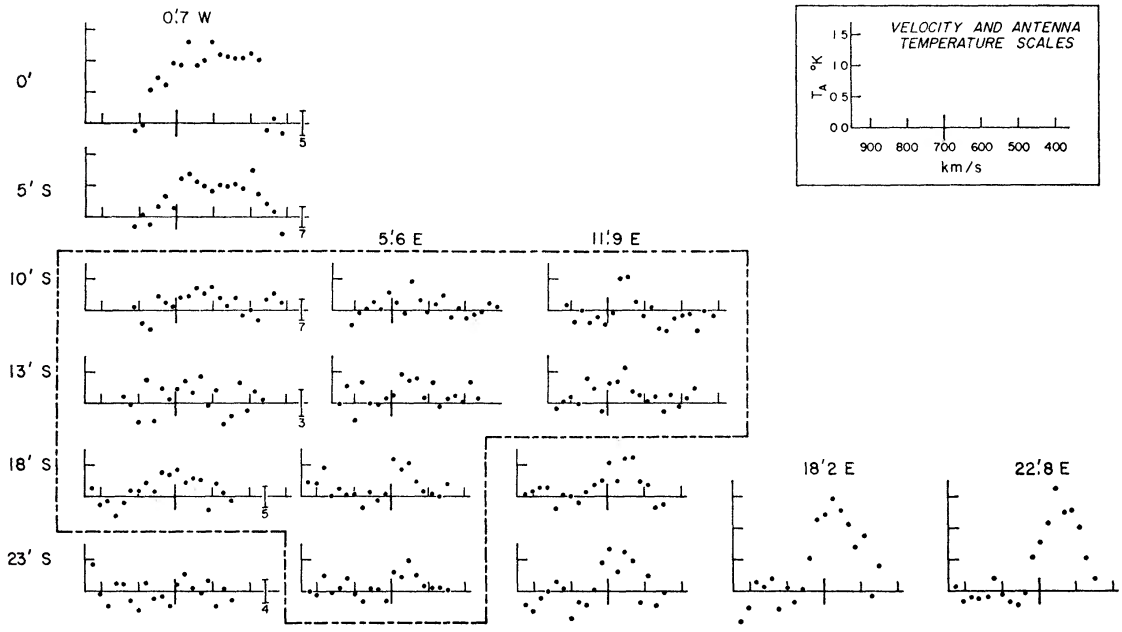

FIG. 5.—Velocity profiles from the center of NGC 4631 through the bridge region and to the center of NGC 4656. The bridge region is outlined by dashed lines. The heavy vertical line on the velocity axis of each profile corresponds to 700 km/s. The number of observations at each declination is noted under the error bars. All positions are with respect to the optical center of NGC 4631.

profile is approximately constant in shape with $T_a \simeq 1°$ K over a velocity range of ~ 470 to ~ 700 km/s (all velocities are with respect to the Sun). At 5′ south, the shape is similar with an amplitude of $\sim 0.5°$ K. This is consistent with an expected line-shaped source of radiation located at the half-power point of the beam. At a full beam width south, a line source would have a peak temperature of $\sim 0.06°$ K, the shape of the profile remaining the same. The observed velocity profile has a peak value of $\sim 0.25°$ K and is narrower than the profile at the center declination. The observed profile at 13′ south has the fewest number of observations in this series and has the poorest signal-to-noise ratio. Nevertheless, a signal of $\sim 0.2°$ K is suggested. At 18′ south the velocity profile is still strong and quite different in shape from the central declination profile.

The other velocity profiles in the region of the bridge show similar velocity and temperature differences from that expected from antenna beam effects alone. The possibility that an unrecognized secondary lobe is present is also unlikely because of the requirements on *both* signal size and velocity profile shape. It is thus quite improbable that the bridge is due to instrumental smearing.

Most of the velocity profiles in the bridge are centered at ~ 650 km/s and have a total width of ~ 100 km/s. The velocity profiles along the major axes of NGC 4631 (Fig. 3) and NGC 4656 (Fig. 4) show the systematic variation expected for rotating systems. The sections of the two galaxies nearest one another in right ascension are receding at approximately the same velocity.

VI. ROTATION CURVE

The beam widths of presently available filled aperture radio telescopes are larger than or at least a significant fraction of the angular size of most galaxies. The presence of ordered motions within a galaxy allows a separation of different regions through their different radial velocities, and a narrow-beam antenna can fix rather accurately the centroid of the radiating hydrogen at a particular velocity. The location of this centroid is determined by a variety of factors, some observational and some intrinsic to the galaxy. All these factors must be taken into account in attempting to derive the rotation curve of a galaxy from the centroid or any other measure of a drift curve or velocity profile. In this section a procedure is outlined in which the entire shape of a drift curve (or velocity profile) is used to obtain the rotation curve.

The observed shape of a drift curve measured at velocity V centered in the velocity interval $\pm \Delta V/2$ is determined by the following factors:

a) Galaxian properties
   1. Rotation curve
   2. Distribution of neutral hydrogen
   3. Random motions (which may include large-scale ordered deviations from the rotational motion)

b) Orientation and motion in space
   1. Inclination
   2. Position angle
   3. Systemic radial velocity

c) Instrumental parameters
   1. Beam size and shape
   2. Velocity width of filter

Given the instrumental parameters, we wish to determine the orientation, motion, and intrinsic properties of a galaxy from a set of drift curves (or velocity profiles). The approach adopted here is to construct a simplified but reasonable model of a galaxy, orient it in space, convolve it with the antenna beam and a set of velocity filters, and compare the resultant drift curves with the observed drift curves. A best but not necessarily unique set of values for (*a*) and (*b*) above will then give the best fit to the observed

drift curves. Here, the closeness of fit is measured by the rms of the deviations, observed *minus* computed, evaluated every 10 sec (time) along the drift curves. The observed drift curves were first smoothed before the comparison was made. The broadening effects of this smoothing, as well as those due to the time constant of the receiver, were taken into account in the model calculations.

The rotation curve is approximated by a form suggested by Brandt (1960):

$$V_C = \frac{AR}{(1+R^nB^n)^{3/2n}}, \tag{2}$$

where V_C is the circular velocity at the radial distance R measured in the plane of the galaxy. The quantities n, A, and B are constants for any particular rotation curve. The maximum of the rotation curve (V_m, R_m), is related to A, B, and n by

$$A = \frac{V_m 3^{3/2n}}{R_m} \quad \text{and} \quad B = \frac{2^{1/n}}{R_m}. \tag{3}$$

The model-fitting program has as input V_m, R_m, and n.

The neutral hydrogen is taken to lie wholly in the plane of the galaxy. The distribution is approximated by a two-component model of a concentric ring and disk, i.e., a distribution which has a minimum in the center. This distribution is described by four parameters: the ring radius, $R_{\rm H}$, ring half-thickness, $\sigma_{\rm H}$ (the cross-section of the ring is taken to be Gaussian), the disk radius, $D_{\rm H}$, and the percentage, P, of the total hydrogen to be associated with the ring distribution. A ring-shaped hydrogen distribution is adopted since this is a common feature in the gross H I distribution for intermediate and late-type spirals (Roberts 1967).

The random motion term, σ_V, includes random motions with respect to a regional standard of rest, as well as any large-scale (possibly ordered) deviations from the rotational motion. An additional feature of the model generating program allows an expansion (or contraction) term, E, to be added to the rotation equation. The radial velocity is then given by

$$V_r = V_C \sin i \cos\theta + E \sin i \sin\theta + S, \tag{4}$$

where i is the inclination, S the systemic velocity, and θ the angular distance from the major axis. The expansion term can be taken either as constant or varying with R, i.e., $E = C_1$, C_2/R, or C_3/R^2. The signs of V_C, i, and E fix the sense of rotation, inclination, and expansion (i.e., expansion or contraction). With the condition that spiral arms trail, the signs of V_C and i may be fixed for a system where the winding of the arms is visible. This is not possible for NGC 4631 and a distinction between expansion and contraction cannot be made since E and $\sin i$ occur as a product in equation (4). This ambiguity exists in the "expansion" solutions discussed below.

Thus, a model drift curve or velocity profile is determined by twelve parameters, the beam shape and filter width being fixed. For NGC 4631, the position angle and inclination were also taken as known. The remaining ten parameters are V_m, R_m, n, $R_{\rm H}$, $\sigma_{\rm H}$, $D_{\rm H}$, P, σ_V, E, and S. Since drift curves for a variety of velocities (and the equivalent: velocity profiles for a variety of positions) are available from the observations, the model parameters may be evaluated at various parts of the galaxy. In the present case fifteen drift curves were used and some sixty models were tested. Five of the drift curves showed very poor fits. The remaining ten converged to the same set of model parameters, although several of these drift curves showed better fits for slightly different combinations of parameters. The adopted model was that with the smallest over-all average rms. The parameters of this model are listed in Table 2. All fifteen of the drift curves are shown in Figure 6 along with the theoretical drift curves produced by the model of

TABLE 2

PARAMETERS OF BEST-FITTING MODEL FOR NGC 4631

Position angle (adopted)	87°
Inclination (adopted)	85°
Systematic radial velocity	630 ± 10 km/s (est. error)
V_m (maximum of rot. curve)	140 (130)* km/s
R_m (maximum of rot. curve)	8′ (7′–10′)*
n (see eq. [2])	3 0 (1 5–3 0)*
R_H (H I ring radius)	5′.6
σ_H (H I ring half-width)	2′.2
D_H (H I disk radius)	11′.0
P (percentage of H I in ring)	66 0
σ_V ("random" motion)	30 0 km/s
E (expansion term)	0†

* Other possible values showing a good fit.

† See text.

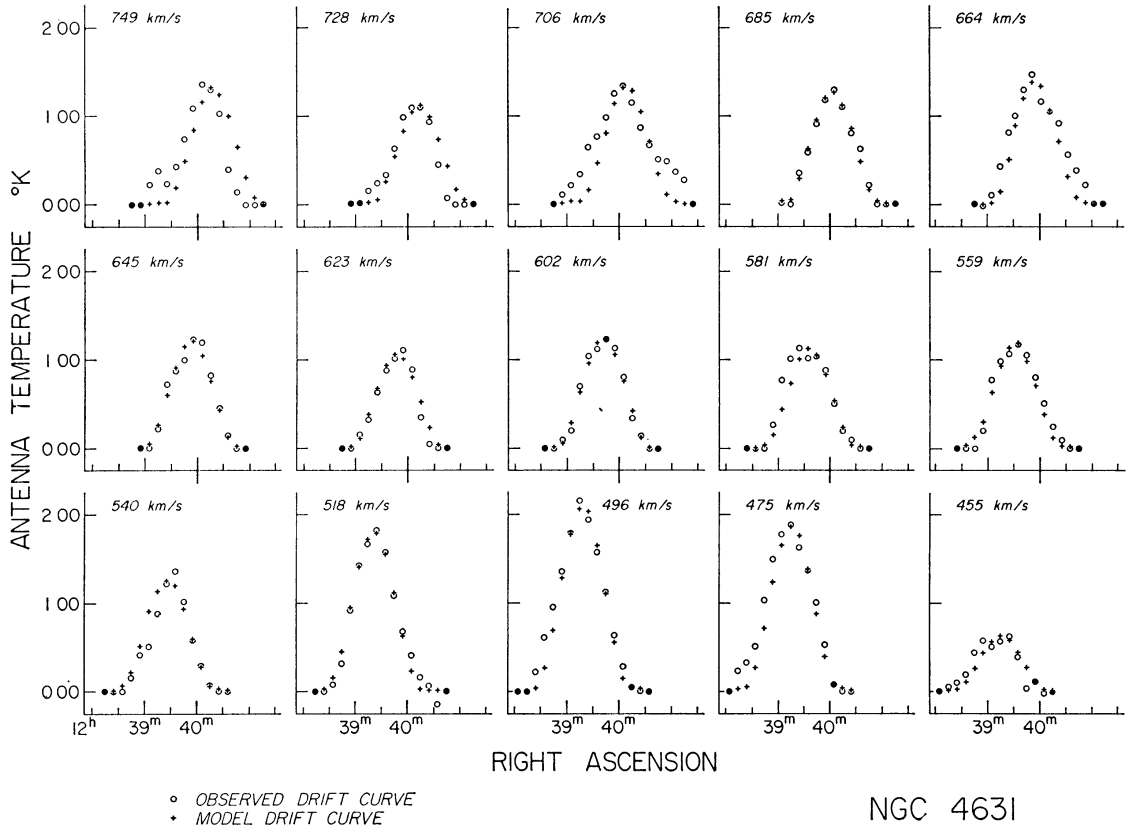

FIG. 6.—The 15 drift curves used in the model-fitting program for NGC 4631. Both the smoothed observed drift curves and the calculated drift curves are shown.

Table 2. Half of the drift curves showed better fits with hydrogen distributions different from that adopted; no systematic variation in the H I model distribution was evident for these drift curves. Such differences would indicate structure in the highly simplified uniform ring-disk distribution adopted here. One interesting result is the large random motion term. The over-all best-fitting model requires $\sigma_V = 30$ km/s. An expansion (or contraction) term did not improve the over-all fit, although it did significantly improve four of the five highest velocity drift curves; these velocities are associated with the east end of the galaxy. The model fitting for NGC 4631 was found to be relatively insensitive to small changes in V_m, R_m, and n. Other possible values for these quantities are included in parentheses in Table 2. No attempt was made to fix the uncertainty of the remaining parameters.

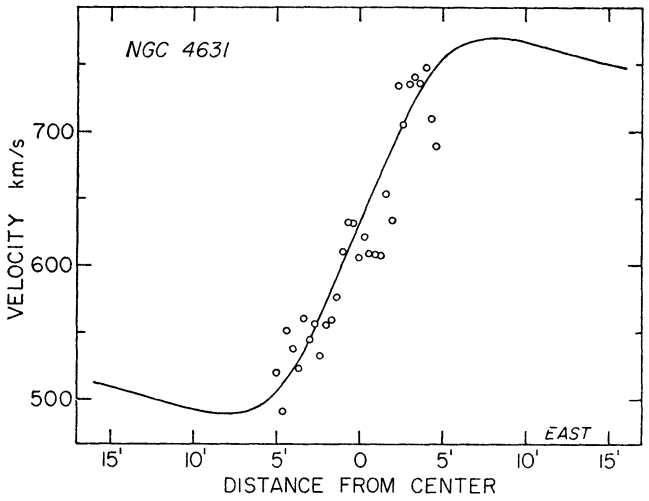

FIG 7

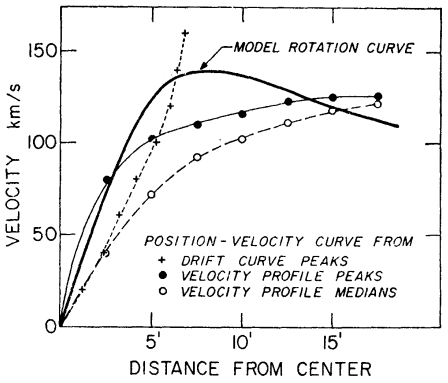

FIG 8

FIG. 7.—The best-fitting rotation curve derived from the model-fitting program. The open circles are optical measurements of NGC 4631 made by de Vaucouleurs and de Vaucouleurs (1963).

FIG. 8.—Comparison between a model input rotation curve and position-velocity curves derived from drift curves and velocity profiles. The heavy solid line represents the input rotation curve for a program which generates drift curves and velocity profiles. The other curves show the effects of beam smearing on "rotation curves" derived from these drift curves and velocity profiles.

Figure 7 shows the adopted rotation curve. Also shown in this figure are radial velocities for various points along the major axis from optical measurements by de Vaucouleurs and de Vaucouleurs (1963, Table 5). Since NGC 4631 is seen almost edge-on, these values are essentially those of the circular velocity. A westward shift of 110″ has been made to the optical data, which were measured with respect to an arbitrary bright feature in the optical image of the galaxy.

It is of interest to note the form of the "rotation curve" if one uses a directly measured parameter of the drift curves or velocity profiles. Such a procedure has been used in the past for several galaxies where the ratio of galaxy size to beam size was of the order of 2 or less.

The parameters that are most frequently used are (1) locations of the peaks of individual drift curves; (2) locations of the peaks of individual velocity profiles; and (3) locations of the median values of individual velocity profiles. We shall refer to curves derived from such data sets as "position-velocity curves" (p-v curves). The model-fitting program generates drift curves and velocity profiles from which p-v curves may be constructed. This has been done for the model described in Table 2. Shown in Figure 8 are

the resultant p-v curves, together with the rotation curve serving as input to the model. It is obvious from this figure that p-v curves give a very poor approximation to the rotation curve when the ratio of galaxy size to beam size is so unfavorable.

The computed drift curves are normalized to the areas inclosed by the observed drift curves, and a normalization to the peak values (an average of the three highest points) is also computed. A set of such normalization factors indicates the relative distribution of hydrogen within the model as compared with that in the galaxy. For a given drift curve a normalization factor larger than the average indicates more hydrogen in that part of the galaxy than allowed for by the model. Figure 9, *a*, shows the run of (area) normalization factors for the final model of NGC 4631. They are all relatively constant

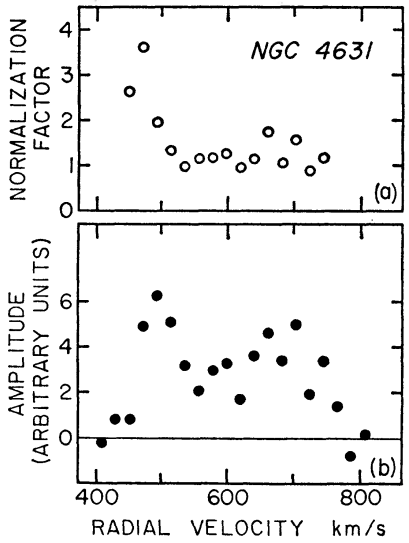

FIG. 9.—(*a*) The run of normalization factors required to match the areas of model drift curves to the observed drift curves This figure shows the relative distribution of neutral hydrogen compared with the adopted model distribution. A large normalization factor indicates an overabundance of H I in the galaxy at that velocity. (*b*) The observed velocity profile for the entire galaxy. The data refer to all 20 channels, of which only 15 show significant signals.

except for the first three which are large and indicate an excess of H I in the galaxy at these velocities compared with the over-all model. This "excess" hydrogen is also seen in Figure 3 where the low-velocity hydrogen appears as quite a strong signal for the west end of the system. This feature may be similar to the hydrogen concentration at the southwest end of M31 (Burke, Turner, and Tuve 1964; Roberts 1967). Figure 9, *b*, shows the over-all velocity profile for NGC 4631. The points in this figure are the sums, along the time axis, of each drift curve; the vertical scale is arbitrary.

The total mass of a system whose rotation curve is of the form of equation (2) is given by (Brandt 1960):

$$\frac{M_t}{M_\odot} = 72.6\left(\tfrac{3}{2}\right)^{3/n} D R_m V_m^2 , \qquad (5)$$

where the distance, D, is in megaparsecs, R_m is in arc minutes, and V_m is in km/s. Allowance for a system of finite thickness is included in the constant term. The model parameters in Table 2 yield a value of $6.8 \times 10^{10}\ M_\odot$. The uncertainty in the mass due to uncertainties in V_m, R_m, and n gives a range of $(4.4\text{–}12.8) \times 10^{10}\ M_\odot$. Various derived and adopted parameters of NGC 4631 are summarized in Table 3.

VII. OPTICAL DEPTH

Epstein (1964) has computed optical depths for galaxies of high inclination. His calculations, based on a highly simplified model, showed that the assumption of small optical depth usually made in deriving the total atomic hydrogen content of a galaxy is not valid for galaxies of high inclination. The rotation curve and hydrogen distribution derived for NGC 4631 allow a more realistic, but still approximate, determination of the average optical depth of this system. We first require a value for the brightness temperature, T_B, which may be obtained from the observed antenna temperature. The necessary relation is

$$T_B = \frac{1}{\eta_B} \frac{\Omega_M}{\Omega_s} T_A , \tag{6}$$

where η_B is the beam efficiency and Ω_M and Ω_s are, respectively, the main beam solid angle and the effective source solid angle (Baars, Mezger, and Wendker 1965). For a velocity interval $\pm \Delta V$, about V, the effective solid angle is

$$\Omega_s(V) = \int\int S(\xi,\zeta,V) A(\xi,\zeta) d\xi d\zeta \tag{7}$$

for a brightness distribution given by $T_B(\xi,\zeta,V) = T_B S(\xi,\zeta,V)$ and a similarly normalized antenna power pattern $A(\xi,\zeta)$.

TABLE 3

SUMMARY OF PROPERTIES OF NGC 4631

Distance	4 0 Mpc
Systemic radial velocity (with respect to Sun):	
Optical (de Vaucouleurs and de Vaucouleurs 1963)	630 km/s
21 cm	630 ± 10 km/s
Structural type:	
Sandage (1961)	Sc
de Vaucouleurs and de Vaucouleurs (1964)	SB(s)d
Morgan (1958)	af:S7 or aI
Photographic magnitude (Holmberg 1958)	9 71
Color index (Holmberg 1958)	0 42
Optical dimensions (Holmberg 1958)	$19' \times 4.'4$
C_0 (color corrected for inclination and galactic extinction)	0 32
L_0 (photographic luminosity corrected for inclination and galactic extinction)	$9\ 6 \times 10^9\ L_\odot$
$M_{\mathrm{H\,I}}$ (neutral atomic hydrogen mass)	$4 \times 10^9\ M_\odot$
M_t (total mass)	$6.8 \times 10^{10}\ M_\odot$
$M_{\mathrm{H\,I}}/L_0$	0 42
$M_{\mathrm{H\,I}}/M_t$	0 06
M_t/L_0	7 1

To evaluate equation (7) we require the distribution of H I as a function of radial velocity. A radial velocity map is easily constructed from the rotation curve and inclination. Such a map, based on the model parameters of Table 2 and displaying the loci of constant radial velocity, is shown in Figure 10. Only one-half of the map is drawn since the rotation curve is assumed to by symmetrical. The minor axis corresponds to the systemic velocity and has been set to zero; the other loci are spaced by 20 km/s. An optical outline based on Holmberg's (1958) values for the major and minor axes is indicated as the outer half-ellipse.

The ring component of the hydrogen distribution is shown in Figure 10 as a shaded area. The width of this ring along the major axis is $2\sigma_{\mathrm{H}}$. The disk component is not

shown; it would appear as an elliptically shaped outline (corresponding to an inclination of 85°) with a semimajor axis of 11′. The combination of velocity loci and hydrogen distribution defines the source size and shape, $S(\xi,\zeta,V)$, for various radial velocity intervals. Two approximations have been made in evaluating equation (7): (*a*) that the brightness temperature is constant over the ring and the disk distributions and corresponds to the model solution which requires 66 per cent of the hydrogen in the ring; (*b*) that the antenna response is constant over a given velocity interval. This latter approximation is reasonable for NGC 4631 since the source size is small with respect

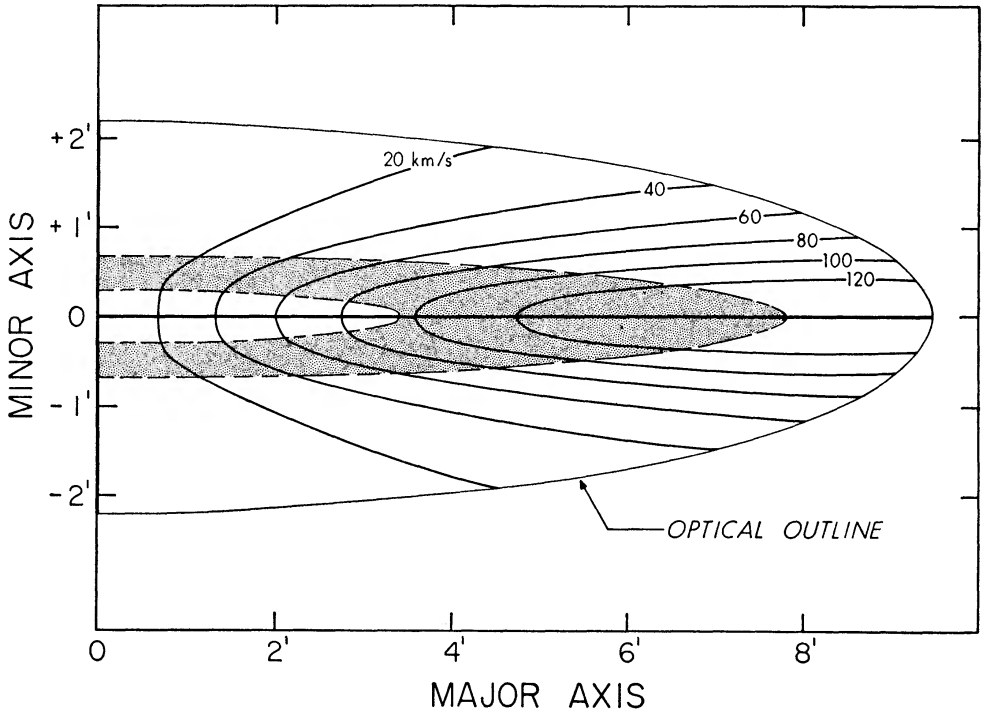

FIG. 10.—The V-shaped curves represent lines of constant radial velocity for NGC 4631. The minor axis corresponds to the systemic radial velocity, here set equal to zero. The other loci are labeled with their appropriate differential radial velocity. The shaded area represents the "ring" component of the neutral hydrogen distribution in this system; the disk component is not shown. Only one-half of the galaxy is displayed since the rotation curve and hydrogen distribution are assumed to be symmetric about the center.

to the beam half-width. The velocity interval determining the source size is given by the filter width plus twice the random motion term, σ_V. As an example, consider the 80 km/s locus in Figure 10. For a filter width of $\pm$ 10 km/s and σ_V = 30 km/s, the source size is fixed by the velocity interval 80 $\pm$ 40 km/s, i.e., the loci 40 km/s and 120 km/s. The size and shape of the ring component contribution is then immediately evident from Figure 10.

Figure 10 and a similar figure for the disk distribution were used to numerically evaluate equation (7). For σ_V = 30 km/s, the resultant average brightness temperature for all filters is T_B = 60° K; this value will be used to evaluate τ. (For comparison, T_B was also derived for the case σ_V = 10 km/s; the average value of T_B is 115° K.) The optical depth is given by

$$\tau = -\ln\left(1 - \frac{T_B}{T_S}\right), \tag{8}$$

where T_S is the spin temperature. Adopting $T_S = 125°$ K, we find $\langle\tau\rangle = 0.65$. This value of the optical depth is the average over all the velocity filters and may be used to correct the total H I mass derived in § IV. The correction factor, C, in equation (1) is

$$C = \langle\tau\rangle/(1 - e^{-\langle\tau\rangle}) . \quad (9)$$

For $\langle\tau\rangle = 0.65$, $C = 1.35$, and the corrected hydrogen mass is $M_{\text{H I}} = 4.0 \times 10^9\ M_\odot$.

The assumption of small optical depth is implicit in the model galaxy program described above. Such an assumption is valid for low-inclination galaxies and is also reasonable for NGC 4631 for the above value of $\langle\tau\rangle$. This would not be the case for a significantly larger optical depth, and the question may be raised of circularity of argument in using the results of an optically thin model to compute optical depths. The most significant factor entering the above calculation for optical depth is σ_V (the use of $\sigma_V = 10$ km/s for NGC 4631 would indicate $\langle\tau\rangle = 2.5$ compared to $\langle\tau\rangle = 0.65$ for

TABLE 4

SUMMARY OF PROPERTIES OF NGC 4656

Distance	4.0 Mpc
Systemic radial velocity (with respect to Sun):	
Optical (Humason *et al.* 1956)	721 ± 63 (A.D.) km/s
21 cm	600 ± 30 km/s
Structural type:	
Sandage (1961)	Irr I
de Vaucouleurs and de Vaucouleurs (1964)	SB(s)mp
Morgan (1958)	aI
Photographic magnitude (Holmberg 1958)	10 74
Color index (Holmberg 1958)	0.24
Optical dimensions (Holmberg 1958)	14′.5 × 4′.1
L (photographic luminosity corrected for galactic extinction only)	$1\ 4 \times 10^9\ L_\odot$
$M_{\text{H I}}$	$1\ 4 \times 10^9\ M_\odot$
M_t	$1\ 5 \times 10^{10}/M_\odot \sin^2 i$
$M_{\text{H I}}/L$	1 0
$M_{\text{H I}}/M_t$	$0\ 09 \sin^2 i$
M_t/L	$11/\sin^2 i$

$\sigma_V = 30$ km/s). Since a large random motion component will not be masked by a large optical depth, the problem becomes one of the accuracy with which σ_V may be determined. For NGC 4631 there is a clear variation in the matching of model to observed drift curves as σ_V is changed. The lowest rms deviation occurs at 30 km/s and becomes systematically larger for both smaller and larger values of σ_V. The range of variation about the minimum value is from 14 per cent, for $\sigma_V = 5$ km/s, to 11 per cent for $\sigma_V = 45$ km/s.

The above considerations also show that large random motions can give rise to high antenna temperatures and are therefore more susceptible to measurement. This follows from the fact that for most galaxies the source size in a moderate-width filter, e.g., 100 kHz, is smaller than the antenna half-power beam width (10′). As the random motion component gets larger, so will the size of the radiating source as seen in such a filter. This will result in less beam dilution, and for a given brightness temperature will yield a higher antenna temperature (see eq. [6]).

VIII. NGC 4656

The velocity profiles at different positions along the major axis of NGC 4656 show a systematic variation in shape suggestive of rotation (see Fig. 4). However, attempts at

model fitting were inconclusive and no single set of parameters satisfying more than three or four of the sixteen drift curves tested could be found. The model drift curves are strongly dependent on two parameters: (1) the sense of the inclination, i.e., whether a given half of the minor axis is tipped toward or away from the observer; and (2) large changes in the systemic velocity, e.g., changes larger than 20 km/s. A systemic radial velocity for NGC 4656 as large as +721 km/s, the optically measured value (Humason, Mayall, and Sandage 1956) for a point 18″ west of the center, is not consistent with any of the drift curves. A value of 600 ± 30 km/s is suggested from the present data. The relatively large uncertainty results from the inability to derive an over-all model for the galaxy.

Individual drift curves required completely different inclinations covering a range of +10° to −60°. There is some suggestion that the inclination varies along the major axis. A centrally concentrated hydrogen distribution rather than a ring distribution generally gave better fits to the observed drift curves.

No rotation curve could be derived, and only the roughest estimate of the total mass is possible. A p-v diagram constructed from the velocity profiles yields estimates of (V_m) sin i and R_m. From equation (5) with $n = 3$, we obtain $M_t/M_\odot = 1.5 \times 10^{10}/\sin^2 i$ (if a unique inclination for NGC 4656 exists). Other properties of NGC 4656 are summarized in Table 4.

I am indebted to Kurtiss J. Gordon for preparing and programing for computer the model-fitting analysis technique.

REFERENCES

Arp, H. C. 1966, *Atlas of Peculiar Galaxies* (Pasadena: California Institute of Technology).
Baars, J. W. M., Mezger, P. G., and Wendker, H. 1965, *Ap. J.*, **142**, 122.
Bergh, S. van den. 1960, *Ap. J.*, **131**, 558.
Bok, B. J. 1966, *Ann. Rev. Astr. and Ap.* (Palo Alto, Calif.: Annual Reviews), **4**, 95.
Brandt, J. C. 1960, *Ap. J.*, **131**, 293.
Burke, B. F., Turner, K. C., and Tuve, M. S. 1964, *Annual Report of the Director, Dept. of Terrestrial Magnetism, 1963–1964* (Washington, D.C.: Carnegie Institution of Washington), p 341.
Epstein, E. 1964, *A.J.*, **69**, 521.
Heeschen, D. S. and Wade, C. M. 1964, *A.J.*, **69**, 277.
Hindman, J. V., Kerr, F. J., and McGee, R. X. 1963, *Australian J. Phys*, **16**, 570.
Höglund, B., and Roberts, M. S. 1965, *Ap. J.*, **142**, 1366.
Holmberg, E. 1958, *Lund Medd.*, Ser. 2, No. 136.
Humason, M. L., Mayall, N. U., and Sandage, A. R. 1956, *A.J.*, **61**, 97.
Morgan, W. W. 1958, *Pub. A.S.P.*, **70**, 364.
Roberts, M. S. 1963, *Ann. Rev. Astr. and Ap.* (Palo Alto, Calif.: Annual Reviews), **1**, 149.
———. 1966, *Phys Rev. Letters*, **17**, 1203
———. 1967, *Proc I.A.U. Symp.*, No. 31, Radio Astronomy and the Galactic System, ed. H. van Woerden (London: Academic Press), Paper 32.
Sandage, A. R. 1961, *Hubble Atlas* (Washington, D.C.: Carnegie Institution of Washington).
———. 1962, I.A U. Symp. No 15, *Problems of Extragalactic Research*, ed. G. C. McVittie (New York: Macmillan Co), p. 359.
Sersic, J. L. 1960, *Zs f. Ap.*, **50**, 168.
Vaucouleurs, G. de. 1968, *Stars and Stellar Systems*, Vol. 9: *Galaxies and the Universe*, ed A and M. Sandage (Chicago: University of Chicago Press) (in press), chap. xvii.
Vaucouleurs, G. de, and Vaucouleurs, A. de. 1963, *Ap. J.*, **137**, 363.
———. 1964, *Reference Catalogue of Bright Galaxies* (Austin: University of Texas Press).